Applied Mathematical Modelling 59 (2018) 233–250

Contents lists available at ScienceDirect

Applied Mathematical Modelling

journal homepage: www.elsevier.com/locate/apm

Optimization of the distribution of small scale linear Fresnel reflectors on roofs of urban buildings

A. Barbón[a], N. Barbón[a], L. Bayón[b,*], J.A. Sánchez-Rodríguez[a]

[a] Department of Electrical Engineering, University of Oviedo, Campus of Gijón, Spain
[b] Department of Mathematics, University of Oviedo, Campus of Gijón, Spain

ARTICLE INFO

Article history:
Received 17 July 2017
Revised 15 January 2018
Accepted 31 January 2018
Available online 9 February 2018

Keywords:
Small-scale linear Fresnel reflector
Urban residential buildings

ABSTRACT

This paper analyses the optimization of the distribution of small-scale linear Fresnel reflectors on roofs of urban buildings. The effects of the two major design parameters (i.e., the form and orientation of the available roof area) on the performance of the reflectors are assessed. We present three new algorithms, related to the classical packing mathematical problem, to develop the optimization method. As decision variables, we use the mirror length and the mirror field width (bounded between upper and lower bounds), jointly with the spacing arrangement of the reflectors. The specific objective is to maximize the collection area considering gaps and shadows. To this end, we will optimize the arrangement, number and dimensions of the reflectors. Finally, we present examples based on real cases and analyse the convergence and accuracy of the algorithms, as well as the required computational effort.

1. Introduction

By 2014, 54% of the world's population was living in urban areas, collectively consuming 75% of global resources; while by 2050, the figure of urban population is forecast to reach 66% [1]. Urban environments are accordingly considered to be important points for the installation of renewable energy technologies. One of the biggest energy consumers in the European Union (*EU*) is the building sector, accounting for more than 40% of the final energy consumption [2]. For this reason, the EU promotes a series of directives to encourage the use of energy from renewable sources in buildings [3]. Furthermore, European standards [4] require new buildings to obtain part of the energy needed for the hot water service from solar sources, depending on the climate zone and the total hot water demand.

There are various renewable energy systems that can be used in the building sector for the production of electricity and heat [5,6]. Solar thermal and photovoltaic systems are currently the most widely used, especially in regions where the annual solar radiation is high, as is the case in the countries of Southern Europe. In these regions, there is a steadily increasing number of installations in the form of domestic solar hot water systems and grid-connected photovoltaic systems. Furthermore, renewable energy systems for space heating and cooling are being developed. Thus, solar energy technologies are called to provide a viable alternative to fossil energy systems.

Solar thermal systems can basically be classified into two types of solar collectors: non-concentrating collectors and concentrating collectors. A non-concentrating collector has the same area for intercepting and for absorbing Sun's beam

* Corresponding author.
E-mail address: bayon@uniovi.es (L. Bayón).

https://doi.org/10.1016/j.apm.2018.01.040

Nomenclature

A	mirror field area (m^2)
AR	aspect ratio
A_T	total mirror field area (m^2)
A_{ar}	available roof area (m^2)
$A_{effe\,i}$	effective area of the absorber tube (m^2)
A_r	roof area (m^2)
a	length of the available roof area (m)
b	width of the available roof area (m)
C_{BC}	building components coefficient
C_{IA}	inclination angle coefficient
C_L	longitudinal component of the reflected radiation
l_{ciai}	length of the circumference illuminated on the absorber tube by the ith mirror (m)
l_a	total illuminated length of the absorber tube (m)
l_s	length step (m)
N	number of reflectors
n	number of mirrors at each side of the central mirror
n_u	optimal number of reflectors
ns_L	number of discretization subintervals used for L
ns_W	number of discretization subintervals used for W
C_{RT}	roof-type coefficient
C_S	shadowing coefficient
C_{Ti}	transversal component of the reflected radiation for the ith mirror ($0 \preceq i \preceq n$)
CL_g	cleanliness factor of the glass
CL_m	cleanliness factor of the mirror
D	diameter of the absorber tube (m)
DNI	direct normal irradiance (W/m^2)
d	separation between two consecutive mirrors (m)
eb, $e'b$	terrace boundary distances (m)
e_h	transversal maintenance distance (m)
e_v	longitudinal maintenance distance (m)
F_r	roof form
f	height of the receiver (m)
IAM	incidence angle modifier
L	reflector length (m)
L_M	length of the mirrors (m)
L_a	length of the single absorber tube (m)
L_i	position of ith mirror ($0 \preceq i \preceq n$) (m)
L_l	distance between the center of two consecutive reflectors (m)
L_t	distance between the central point of one SSLFR and the starting point of the following SSLFR (m)
μ	angle between the reflected ray and the normal to the NS axis (°)
ρ	reflectivity of the primary mirrors
O_r	roof orientation (°)
Q	total power absorbed (W)
S_t	transversal shading of the absorber tube (m)
t	computing time (s)
W	mirror field width (m)
W_M	mirror width (m)
W_{ai}	width illuminated on the absorber by the ith by mirror (m)
α_b	absorptivity of the material of which the absorber tube is made
α_i	angle between the vertical at the focal point and the line connecting the center point of each mirror to the focal point (°)
α_S	height angle of the Sun (°)
β_a	angle between the absorber tube and the horizontal plane (°)
β_i	tilt of the ith mirror (°)
β_M	angle between the mirror axis and the horizontal plane (°)
γ_S	azimuth of the Sun (°)

η_{opt}	optical efficiency (%)
θ_{IA}	inclination angle for residential roofing (°)
θ_i	angle between the normal to the mirror and the angle of incidence of the Sun (°)
θ_L	lateral incidence angle (°)
θ_l	longitudinal incidence angle (°)
θ_t	transversal incidence angle (°)
θ_z	zenith angle of the Sun (°)
λ	latitude angle (°)
τ	transmissivity of the glass

radiation. In a concentrating collector, the absorbing area is smaller than the intercepting area, thereby increasing the solar radiation. In addition, the operating temperature of both systems is different. The types and characteristics of solar collectors are shown by [7].

There are many studies on the use of flat plate collectors (*FPCs*) in buildings (see, for example [8], [9,10], or [11]). However, there are not many studies on the use of linear Fresnel reflectors (*LFRs*) in buildings. *LFRs* are used, for example, in [12,13], in domestic water heating; in [14], in the heating/cooling of buildings; and in [15], in the absorption air cooled Solar-GAX cycle.

Various *LFR* configurations have been proposed in the literature (see [16]). In the 'conventional' central *LFR*, there are two main blocks: the primary reflector system and the receiver system. The primary reflector system is composed of a frame where rows of mirrors are located. The receiver system consists of one or multiple circular absorber tubes and a receiver cavity, and is located at a certain height from the primary reflector system. In contrast, in the compact linear Fresnel concentrator (*CLFC*) (see [17]), there is a linear absorber at each side of the mirror array so that consecutive mirrors point to different absorbers.

Different configurations of the receiver system have been studied. For example: (i) two linear receivers on separate towers with double row tube arrangements of branch tubes [17]; (ii) a receiver consisting of a bundle of tubes parallel to the mirror array [18]; and (iii) receivers with other optical designs, including circular-cylindrical and parabolic cylindrical mirrors [19].

A small-scale linear Fresnel reflector (*SSLFR*) has the configuration of a 'conventional' central *LFR*. The possibility of longitudinal movement of the *SSLFR* is the main difference with respect to the large-scale *LFR*. In large-scale *LFRs* the study of the device's longitudinal behaviour is not usually performed for two reasons: the absorber size does not permit any configuration allowing the modification of its position, and the influence of the longitudinal position can be considered irrelevant in percentage terms with respect to the total length of the absorber.

The position of the mirrors and the absorber of an *SSLFR* can be adjusted using three different movements (see Fig. 1), as shown in [20] and [21]. First, the mirrors can be rotated on the north-south axis, so as to follow the Sun's daily movement. Second, the mirror row can be rotated on the east-west axis. Finally, the receiver can also be rotated on the east-west axis. A prototype with these characteristics has been manufactured at a vocational training school (CIFP-Mantenimiento y Servicios a la Producción) in La Felguera, Asturias, Spain. These three movements have to be taken into account, especially if several SSLFRs are to be installed on a building roof.

Roofs are optimal locations for *SSLFRs*, as well as for *FPCs*. However, roofs of urban buildings are generally not designed or built to house renewable energy systems. Available roof area has in fact been identified as a major limiting factor in achieving zero energy buildings, especially for taller buildings [22]. The estimation of the roof area has been the subject of many studies, for example: [23–26].

In this paper we analyse the optimization of the distribution of *SSLFRs* on the roofs of urban buildings. In the study, the roof orientation and the available roof area are known parameters. The decision variables are the dimensions of the *SSLFRs* (length and width), which are bounded between upper and lower bounds. In addition, minimum distances between *SSLFRs* are considered in order to allow maintenance and to avoid shadowing effects. As a result of the characteristics of this optimization problem, it can be regarded as new type of two-dimensional rectangle packing problem. Although various types of packing problems have been widely studied, to the best of our knowledge, this particular packing problem has not been addressed in the literature so far.

The paper is organized as follows. The statement of the problem is presented in Section 2, describing the parameters of the *SSLFR* and the roof parameters. Section 3 includes a study of the transversal and longitudinal shadows between *SSLFRs*. The optimization of the distribution of *SSLFRs* on roofs is presented in Section 4, including the description of three different packing algorithms. Section 5 shows numerical results obtained using the three packing algorithms described in the previous section. Finally, Section 6 summarizes the main conclusions of this study.

2. Statement of the problem

In order to estimate the available roof area for the installation of *SSLFRs* (see Fig. 1), several building characteristics have to be taken into account: number, height, construction typologies, orientation, inclination, location, shading, and building

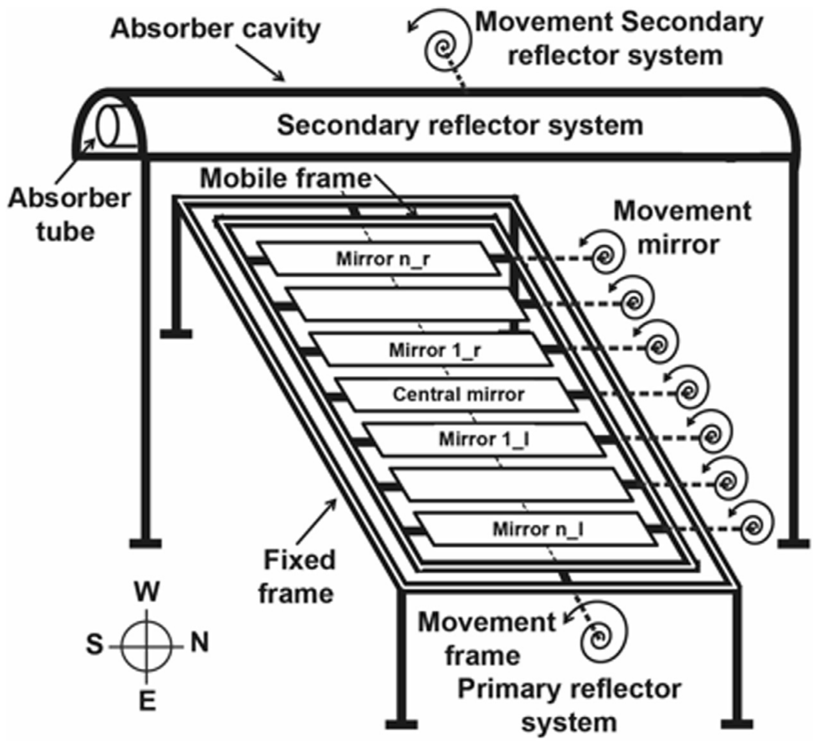

Fig. 1. Schematic of an SSLFR with three movements..

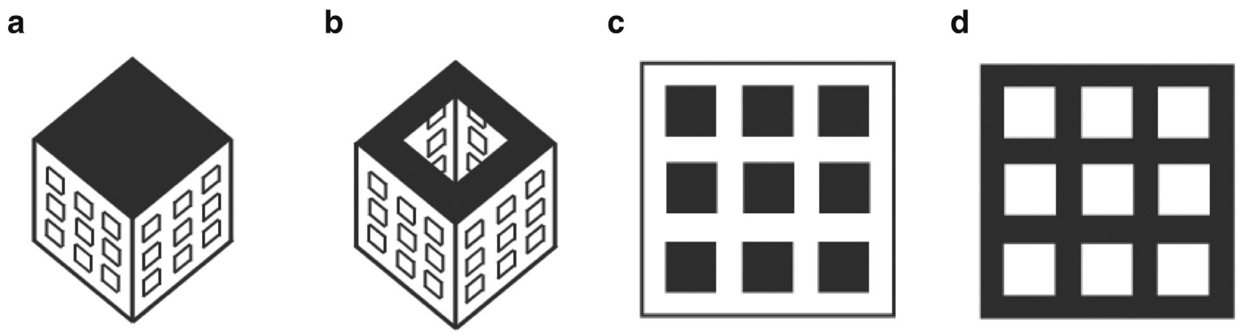

Fig. 2. Simplified urban forms.

components (such as chimneys, elevator machine rooms, fans, and plumbing vents). Due to the complexity of today's urban settings, it is necessary to simplify the different building forms.

To address this problem, [27] analysed two simplified forms: courts and pavilions. A pavilion and a court are shown in Fig. 2(a) and Fig. 2(b), respectively, where black is used for building roofs. Fig. 2(c) and Fig. 2(d) present two archetypal urban patterns with several pavilions and courts, respectively. This division was later used by a large number of studies. Courts and pavilions respectively represent traditional and contemporary building forms, and can be found in many countries.

These two forms from [27] have been subsequently reviewed by [28], resulting in six basic forms (see Fig. 3): (a) Pavilions, (b) Slabs, (c) Terraces, (d) Terrace-courts, (e) Pavilion-courts, and (f) Courts. This paper adopts the pavilion urban form, due to its simplicity and because the calculations can be extrapolated to the remaining urban forms.

Roof inclination is a important parameter for determining the roof area. In urban buildings, roof types are broadly grouped into flat roofs and pitched roofs. Pitched roofs include: the shed roof, gable roof, cross gable roof, saltbox roof, hipped or hip roof, cross hipped roof, gambrel roof, and pyramid roof. Fig. 4 summarizes the established pitched roof typology for generic urban forms: (a) Flat Roof, (b) Shed Roof, (c) Gable Roof, (d) Saltbox Roof, (e) Gambrel Roof, (f) Hipped or Hip Roof, and (g) Pyramid Roof.

The parameters that influence the installation of *SSLFRs* on building roofs are of two types: those intrinsic to the *SSLFR* and those relating to the roof. The potential number of *SSLFRs* to be installed on a roof strongly depend on these parameters.

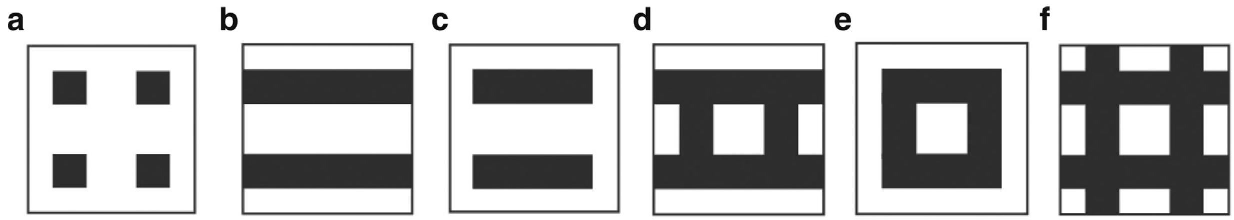

Fig. 3. Generic urban forms.

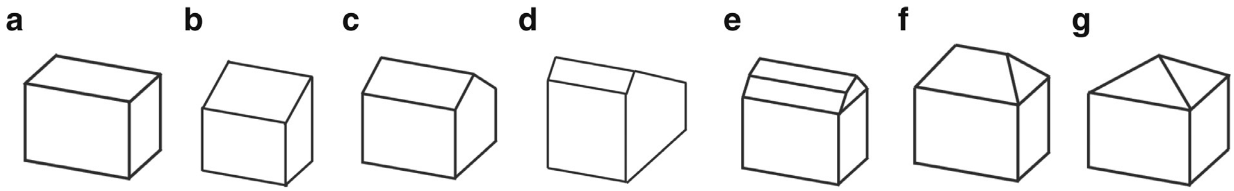

Fig. 4. Roof types for generic urban forms.

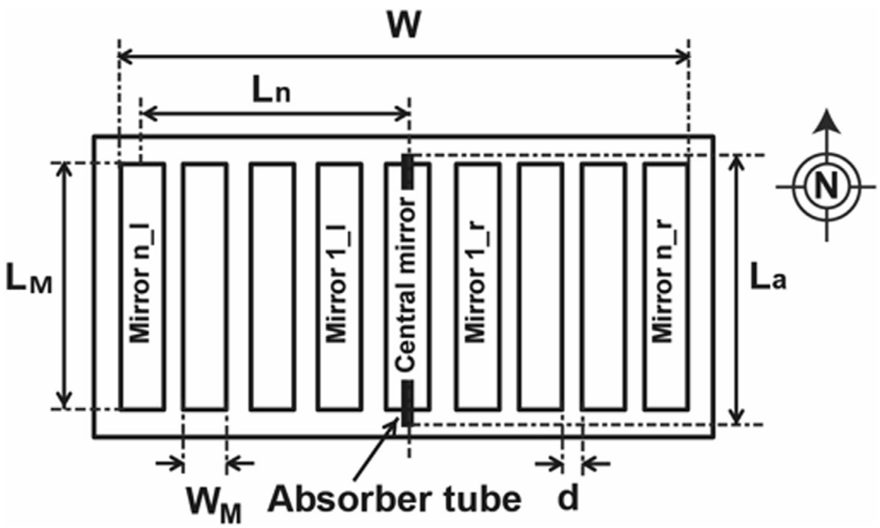

Fig. 5. Parameters of an SSLFR.

2.1. Intrinsic parameters of the SSLFR

These parameters determine the transversal and longitudinal behaviour of the *SSLFR* [20,21]. Considering an *SSLFR* aligned horizontally in a north–south orientation, the angle of incidence of solar radiation will be calculated in two projection planes: the transversal incidence angle (θ_t), and the longitudinal incidence angle (θ_l). The transversal incidence angle (θ_t) is defined as the angle between the vertical and the projection of the Sun vector on the east–west plane (the plane orthogonal to the absorber tube); while the longitudinal incidence angle (θ_l) is defined as the angle between the vertical and the projection of the sun vector on the north–south plane. The relative position of the Sun with respect to the *SSLFR* is determined using the well-known Solpos algorithm [29].

The basic parameters used in the transversal study are as follows: n is the number of mirrors at each side of the central mirror (the total number of mirrors of the *SSLFR* is $2n+1$), W_M is the mirror width, d is the separation between two consecutive mirrors, L_i is the position with respect to the central mirror of the ith mirror ($0 \preceq i \preceq n$), β_i is the mirror tilt of the ith mirror ($0 \preceq i \preceq n$), D is the diameter of the absorber tube, and f is the height of the receiver.

The basic parameters used in the longitudinal study are as follows: β_M is the angle between the mirror axis and the horizontal plane, β_a is the angle between the absorber tube and the horizontal plane, θ_z is the zenithal solar angle, L_M is the mirror length, and L_a is the total length of the single absorber tube.

Fig. 5 shows a ground plan of an *SSLFR*. The mirror field width (W) and the mirror field area (A) can be calculated as:

$$W = 2 \cdot L_n + W_M$$

$$A = W \cdot L_M$$

In order to calculate the energy absorbed by the absorber tube, we will use the equation presented in [21], which is particularly suitable for *SSLFRs*:

$$Q = \sum_{i=0}^{2 \cdot n} DNI \cdot \eta_{opt} \cdot IAM_i \cdot A_{effe\, i},$$

where:

(i) DNI is the direct normal irradiance. In the present study, DNI is discretized every 10 min.

(ii) η_{opt} is the total optical yield, which is calculated considering the reflectivity of the mirrors (ρ), the cleanliness factors of the mirrors (CI_m) and of the glass covering the secondary absorber (CI_g), the transmissivity of this glass (τ), and the absorptivity of the material of which the absorber tube is made (α_b):

$$\eta_{opt} = (\rho \cdot CI_m) \cdot (\tau \cdot CI_g \cdot \alpha_b)$$

Although some of these parameters, especially τ, should change with the angle of incidence (see [30]), in this study they are considered constant for the sake of simplicity (see [31,32]). These values are: $\rho = 0.94$ (see [33]), $CI_m = CI_g = 0.96$ (see [34]), if $\alpha_i \leq 20^o, \tau = 0.87,$ if $20^o \leq \alpha_i \leq 30^o, \tau = 0.85$ (see [30]).

(iii) IAM_i considers the variation in the optical performance of an *SSLFR* for varying ray incidence angles, by the ith mirror, which is calculated using the equation shown by [35]:

$$IAM_i = \left[C_L^2 + C_{Ti}^2 + 2 \cdot C_L \cdot C_{Ti} \cdot \cos \widehat{C_L C_{Ti}} \right]^{1/2}; \quad 0 \leq i \leq 2n,$$

where C_L (common to all mirrors) and C_{Ti} (different for each mirror) are the components of the reflected radiation, the values of which are given by:

$$C_L = \cos \gamma_S \cdot \cos \theta_L; \quad C_{Ti} = \frac{\cos \alpha_S \cdot \sin \gamma_S \cdot \cos \theta_i}{\sin \theta_t}; \quad 0 \leq i \leq 2n$$

(iv) $A_{effe\, i}$ is the effective area of the absorber tube by the ith mirror that is actually illuminated, which is calculated using the equation shown in [35]:

$$A_{effi} = l_{ciai} \cdot l_a; \;\; 0 \leq i \leq 2n,$$

where l_{ciai} is the length of the circumference illuminated on the absorber tube by the ith mirror, and l_a is the total illuminated length of the absorber tube.

A MATLAB code was compiled to trace the Sun's rays. This code uses geometric optics to calculate ray intersections with the primary reflector system. As an example, Fig. 6 presents ray tracing simulations for an *SSLFR*. For the sake of clarity, this visualization shows a reduced number of rays. This simulation was carried out on June 21st (Summer solstice), solar time 10:30, and geographic location: Almeria (Spain), with latitude $36^o 50' 07''$N, longitude $02^o 24' 08''$W and altitude 22 (m).

2.2. The roof parameters

The roof-related parameters are as follows: roof area (A_r), available roof area (A_{ar}), roof form (F_r), and roof orientation (O_r). These parameters are described below.

(1) The available roof area (A_{ar}) is the area that can be used for installing *SSLFRs*. Several authors have applied Geographical Information System (GIS) techniques to determine the available area on roofs of urban buildings (see [23,36,37]). A_{ar} may also be calculated using the following equation:

$$A_{ar} = A_r \cdot C_{BC} \cdot C_S \cdot C_{RT} \cdot C_{IA,}$$

where:

(i) C_{BC} is the building components coefficient, used to take into account components such as chimneys, elevator machine rooms, fans, and plumbing vents. Several studies have concluded that roof-mounted residential building components reduce the available roof area for renewable energy systems to a figure between 21% of the roof [38] and 30% of the roof [25]. Therefore this coefficient can vary between 0.7 and 0.79.

(ii) C_S is the shadowing coefficient, used to correct the shadows caused by other buildings, or by the roof itself. A 3D city model would be necessary to precisely determine this coefficient. It is customary to assume the value found by Izquierdo et al. [23], which is obtained as a function of the representative building typology.

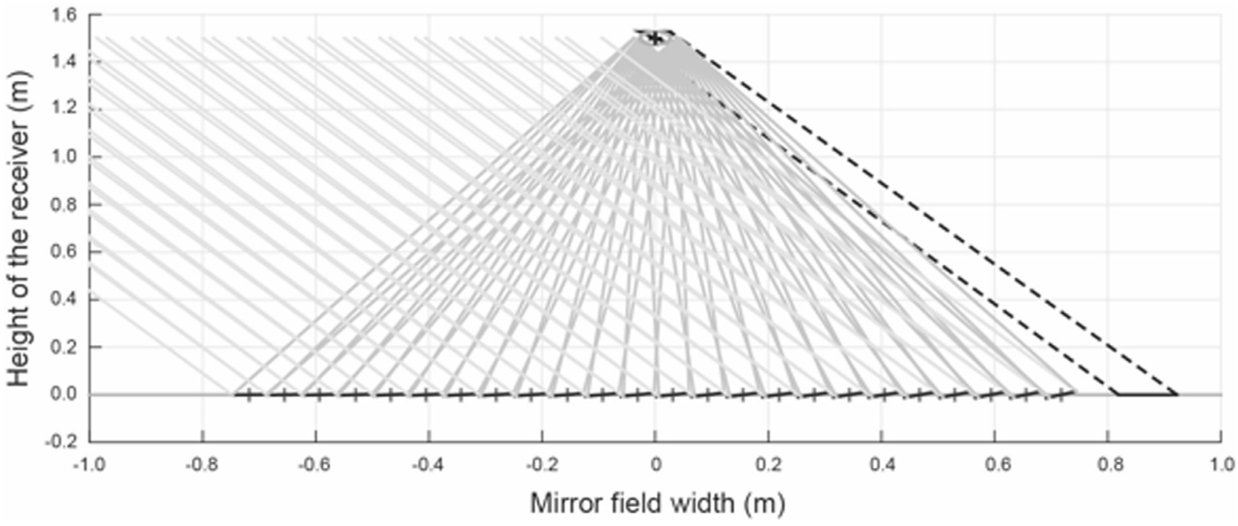

Fig. 6. Ray tracing simulations for an SSLFR.

(iii) C_{RT} is the roof-type coefficient [25]. For flat roofs, $C_{RT} = 1$, while for pitched roofs, this coefficient depends on the number of pitches. If *SSLFRs* are to be installed on only one of the two pitches of the roof, $C_{RT} = 0.5$.

(iv) C_{IA} is the inclination angle coefficient due to the slope of the pitch, and can be calculated as:

$$C_{IA} = \cos(\theta_{IA}),$$

where θ_{IA} is the inclination angle for residential roofing. As an example, the Spanish Technical Building Code [39] states that the slope of the pitch has to be designed in accordance with the roofing material. For a flat roof, $C_{IA} = 1$.

(2) The form of the roof area (F_r) is defined as the ratio between the length (a) and width (b) of the available roof area:

$$F_r = \frac{a}{b}$$

One of the most important ways of characterizing the installation of an *SSLFR* is via its aspect ratio (*AR*), defined as:

$$AR = \frac{W}{L_M}$$

The SSLFR aspect ratio (*AR*) is related to F_r, as F_r imposes a limit to the value of *AR*. The study of this relationship is one of the objectives of this paper.

(3) The roof orientation (O_r) is defined by the angle that forms the north–south direction and the terrace edges. In our study, every *SSLFR* is aligned in the north–south direction and we assume that the terrace edges are parallel to our reference axes ($x - y$). Thus, the roof orientation is given by the angle (α) between the north-south direction and the positive half axis of y.

3. Study of the shadows

This section describes the mathematical method developed to maximize the roof area filled by a set of *SSLFRs*. The objective function to be maximized is the total mirror field area (A_T), given by:

$$A_T = \sum_{i=1}^{N} W \cdot L,$$

where N is the number of reflectors, W is the mirror field width, and L is the reflector length ($L = L_M$). In this study, we assume that all the reflectors are identical in size. The mathematical formulation includes upper and lower bounds for the decision variables W and L, in the following form:

$$W^{\min} \le W \le W^{\max}; \quad L^{\min} \le L \le L^{\max}$$

The optimization model also considers a transversal maintenance distance (e_h) and a longitudinal maintenance distance (e_v), to be kept between reflectors in order to allow proper inspection, cleaning, and maintenance. Moreover, the model evaluates the frontal and lateral shadows between reflectors.

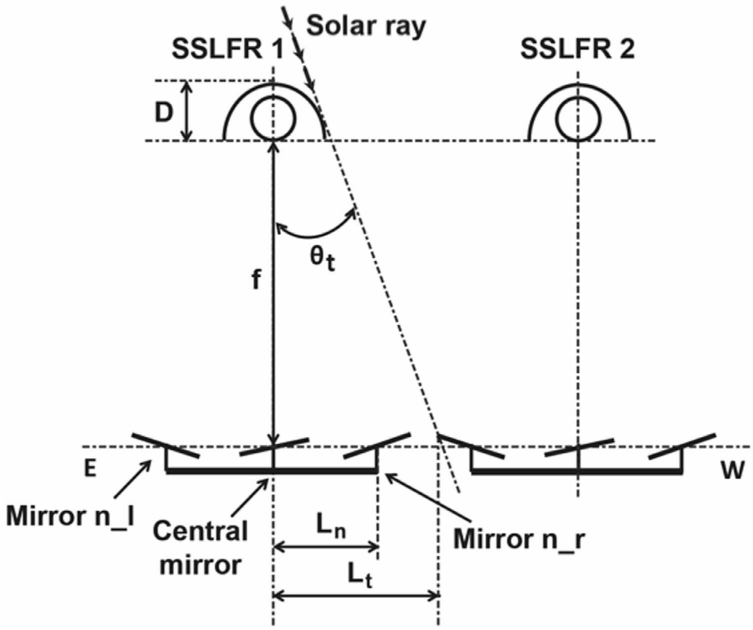

Fig. 7. Transversal shadows.

3.1. Evaluation of the transversal shadow between SSLFRs

As shown in Fig. 7, θ_t is the transversal incidence angle, and L_t is the distance between the central point of one *SSLFR* and the starting point of the following *SSLFR*. Neglecting the effect of the secondary concentrator, L_t is given by:

$$L_t \simeq f \cdot \tan\theta_t$$

The transversal shadow (see Fig. 7) is null provided that the following condition is met:

$$L_t \leq \left(L_n + \frac{W_M}{2}\right),$$

where L_n is the position of the last mirror with respect to the central mirror. When there is a transversal shadow, its value is given by:

$$L_t - \left(L_n + \frac{W_M}{2}\right),$$

The parameters of the *SSLFR* considered here are as follows. Mirror width (W_M): 0.06 (m); vertical distance between the absorber and the mirrors (f): 1.5 (m); mirror thickness: 0.005 (m); mirror length (L_M): 2.0 (m); absorber length (L_a): 2.40 (m); absorber diameter (D): 0.0486 (m); and reflector width (W): 2.076 (m).

The Spanish Technical Building Code [40] states that, in order to minimize shadowing effects, the distance between reflectors has to guarantee a minimum of 4 hours of sunshine around noon on the winter solstice. Applying this standard, on December 21st at 10: 00 the value of L_t is 1.785 (m), as θ_t is equal to -40.05^o. Therefore, there is a transversal shadow of 0.782 (m). For this reason, a transversal maintenance distance (e_h) of 1.0 (m), considered suitable for maintenance purposes, is also sufficient to minimize shadowing effects.

3.2. Evaluation of the longitudinal shadow between SSLFRs

Due to lateral symmetry, we need only take into account the central mirror for this study. Defining L_l as the distance between the centre of two consecutive reflectors, the following relations between angles and distances can be verified (see Fig. 8):

$$L_l^1 = \frac{L_M}{2}\cos\beta_M;\;\; L_l^2 = \left[f + \frac{L_M}{2}\sin\beta_M + \frac{L_a}{2}\sin\beta_a\right]\tan\theta_z$$
$$L_l^3 = \frac{L_M}{2}\sin\beta_M\tan\theta_z;\;\; L_l^4 = \frac{L_M}{2}\sin\beta_M$$
$$L_l = L_l^1 + L_l^2 + L_l^3 + L_l^4$$

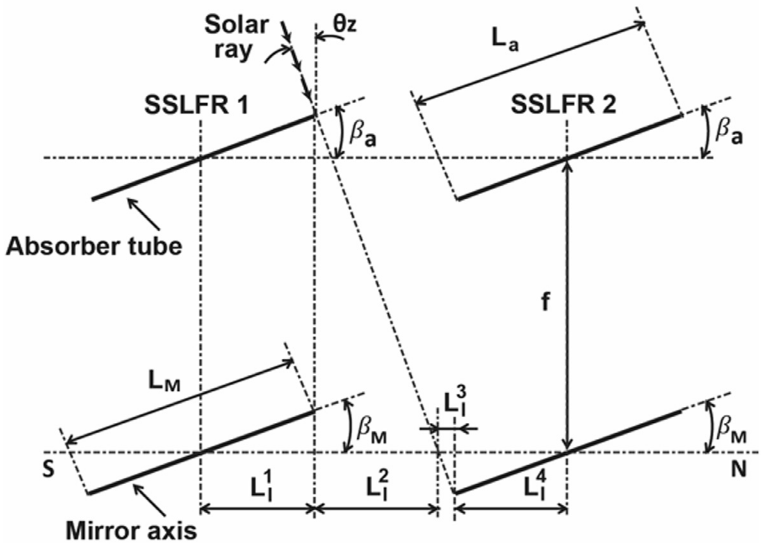

Fig. 8. Longitudinal shadows.

Table 1
Characteristics of the packing problems described in [42].

Problem	1	2	3	4	5	6
Items						
number	n	n	n	*set I*	n	*setI*
width	w_i	w_i	w_i	w_i	w_i	w
height	h_i	h_i	h_i	h_i	h_i	h
				value c_i	*demand* d_i	
Large object						
number	1	1	N (v)	1	N (v)	1
width	W (f)	W (v)	W (f)	W (f)	W (f)	W (f)
height	H (v)	H (v)	H (f)	H (f)	H (f)	H (f)
Objective	min H	min $W.H$	min N	max *value*	min N	max *items*
Packed	n	n	n	*subset I*	n	*subsetI*
					d_i copies	Rotated 90º

When there is lateral shadow (see Fig. 8), its value is given by:

$$L_l^2 + L_l^3$$

Taking into account the Spanish Technical Building Code [40], a longitudinal maintenance distance (e_v) of 1.0 (m), considered suitable for maintenance purposes, is also sufficient to minimize shadowing effects.

4. Optimization of the distribution of SSLFRs on roofs

The distribution of SSLFRs on roofs of urban buildings is optimized in this paper using three new algorithms that are related to the classical mathematical packing problem. Packing problems are a class of mathematical optimization problems that attempt to pack objects into containers [41]. The distribution of SSLFRs on roofs is formulated in this paper as a two-dimensional rectangle packing problem.

Imahori et al. review in [42] several types of rectangle packing problems, as follows: (1) Strip packing problem; (2) Area minimization problem; (3) Two-dimensional bin packing problem ([43,44]); (4) Two-dimensional knapsack problem ([45,46]); (5) Two-dimensional cutting stock problem ([47–49]); and (6) Pallet loading problem [50]. Table 1 summarizes the main characteristics of these problems. The notation (f) indicates a fixed parameter, and (v) a variable.

In computational complexity theory, NP (nondeterministic polynomial time) is a complexity class used to describe certain types of decision problems. Almost all two-dimensional packing problems are known to be NP-hard, and hence it is impossible to solve them exactly in polynomial time. Therefore, heuristic techniques are used to design practical algorithms for these problems.

In this paper we consider a very special type of two-dimensional rectangle packing problem. We have to pack identical rectangles in a fixed rectangle (like, for example, [51]), taking into account additional constraints:

(i) A minimum space must be left between objects for maintenance purposes and to avoid shadowing effects.

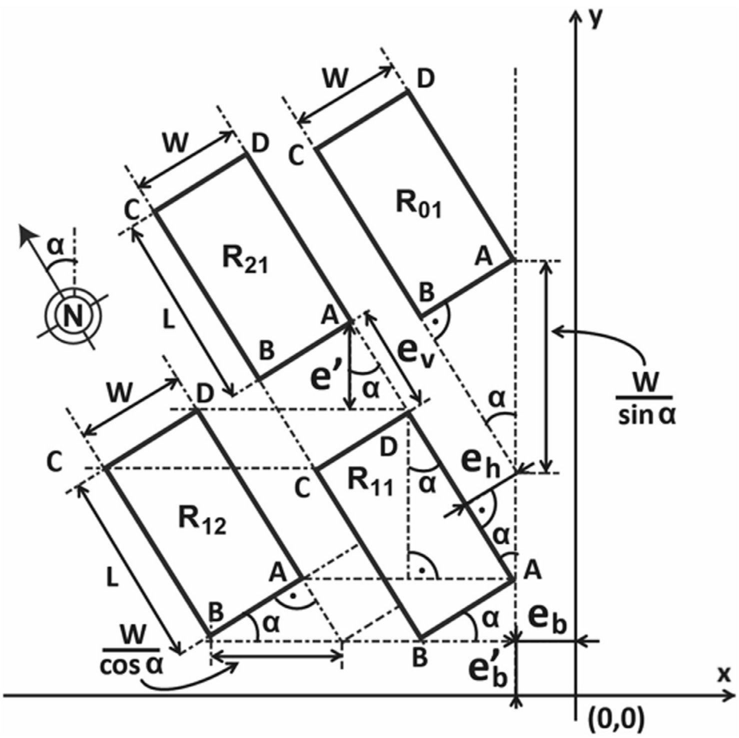

Fig. 9. Type (I) N–S alignment.

Table 2
Optimal values of r for the three types of packing.

$a \times b$		0^o	15^o	30^o	45^o	60^o	75^o	90^o
10×10	I	**0.288**	0.210	**0.224**	0.207	**0.224**	0.210	**0.288**
	II	**0.288**	**0.225**	0.176	**0.210**	0.176	**0.225**	**0.288**
	III	**0.288**	**0.225**	0.201	0.207	0.201	**0.225**	**0.288**
20×10	I	**0.315**	0.245	**0.267**	0.245	**0.243**	0.246	**0.302**
	II	**0.315**	0.224	0.241	**0.247**	0.234	0.262	**0.302**
	III	**0.315**	**0.262**	0.225	0.207	0.241	**0.281**	**0.302**
10×20	I	**0.302**	0.246	**0.243**	0.245	**0.267**	0.245	**0.315**
	II	**0.302**	0.262	0.234	**0.247**	0.241	0.224	**0.315**
	III	**0.302**	**0.281**	0.241	0.207	0.225	**0.262**	**0.315**
30×10	I	**0.336**	0.262	**0.284**	**0.275**	**0.262**	0.257	**0.320**
	II	**0.336**	0.230	0237	0.264	0.249	0.276	**0.320**
	III	**0.336**	**0.275**	0.233	0.230	0.235	**0.288**	**0.320**
10×30	I	**0.320**	0.257	**0.262**	**0.275**	**0.284**	0.262	**0.336**
	II	**0.320**	0.276	0.249	0.264	0.237	0.230	**0.336**
	III	**0.320**	**0.288**	0.235	0.230	0.233	**0.275**	**0.336**

(ii) The orientation of the objects is fixed with respect to the container, and in general they are not orthogonal.
(iii) The dimensions of the objects are not fixed, but they are bounded between upper and lower bounds.

To the best of our knowledge, this packing problem has not been addressed in the literature, therefore we are presenting the first algorithms to solve it.

4.1. Three packing algorithms

In addition to considering the necessary maintenance distances between reflectors, $e_h = e_v = 1.0$ (m), there has to be a minimum distance between the terrace boundary and the reflectors, also for maintenance purposes. These distances are designated eb and $e'b$, and a value of 1 (m) is assumed for both of them. Given a terrace of dimensions $a \times b$, we assume that the terrace edges are parallel to our reference axes $(x - y)$. Let α be the angle between the N–S direction and the positive half axis of y.

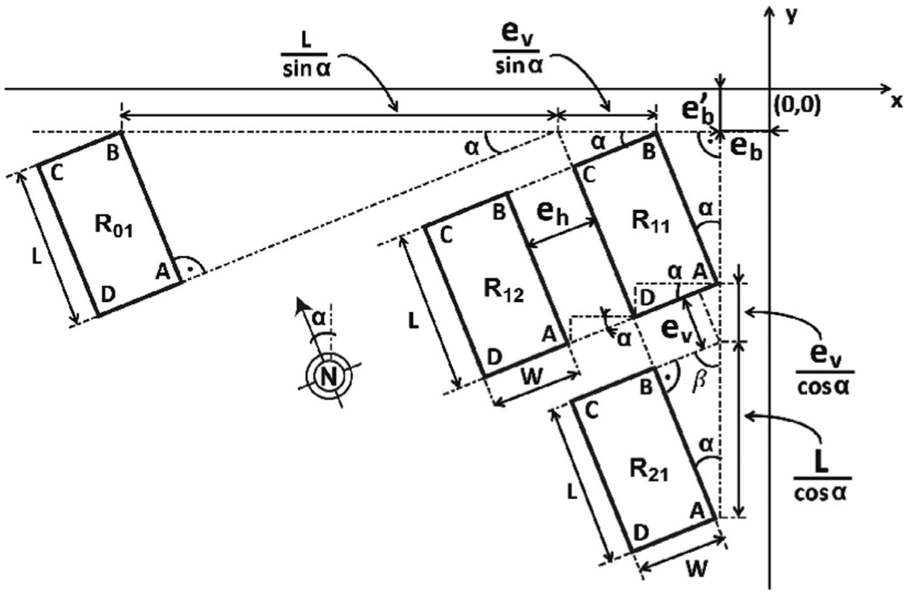

Fig. 10. Type (II) E–W alignment.

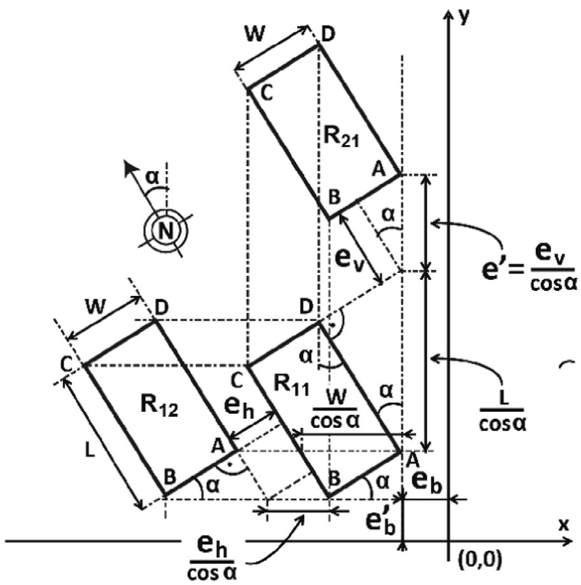

Fig. 11. Type (III-A) X–Y alignment.

As already stated, the problem consists in packing reflectors with length L and width W, these dimensions being bounded between upper and lower bounds. In this paper we will present three different packing schemes in order to solve this packing problem.

TYPE (I) N-S ALIGNMENT

This packing scheme consists of placing rows of reflectors parallel to the north–south direction. In this scheme (see Fig. 9), we define a base rectangle R_{11} using two vertices A and B, which are located as close as possible to the bottom-right corner of the terrace. From the coordinates of these two vertices A and B, the coordinates of the other two vertices C and D can be easily calculated:

$$R_{11}: \begin{cases} A(eb, e'b + W\sin\alpha) & \rightarrow \quad D(x_A + L\sin\alpha, y_A + L\cos\alpha) \\ B(eb + W\cos\alpha, e'b) & \rightarrow \quad C(x_B + L\sin\alpha, y_B + L\cos\alpha) \end{cases}$$

Once the base rectangle R_{11} has been defined, the packing pattern of the first row is completed by placing horizontally, from right to left, as many rectangles R_{1i} as possible, keeping the necessary distances between them. Clearly, the y coordi-

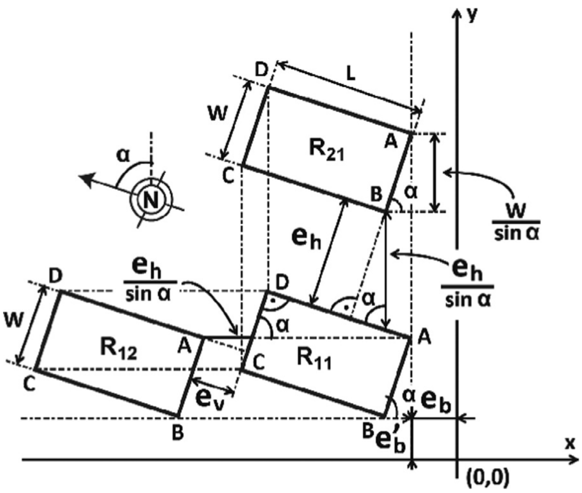

Fig. 12. Type (III-B) X–Y alignment.

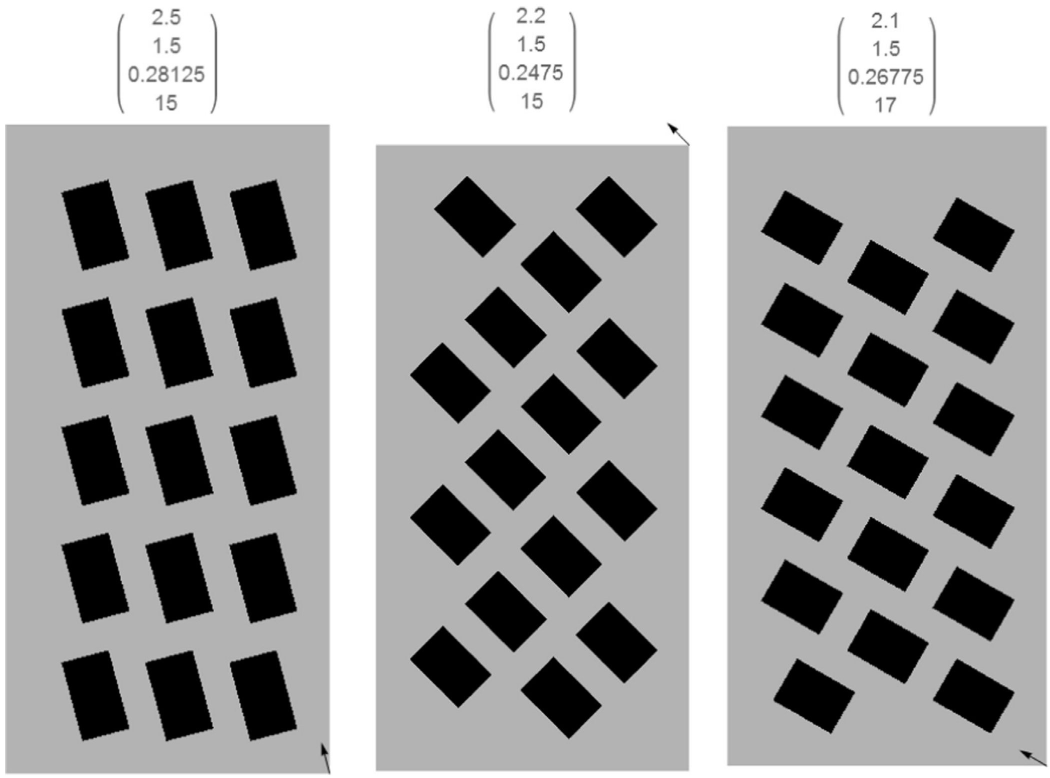

Fig. 13. Optimal solution.

Table 3
Energy absorbed by the absorber tube per year (MWh).

Orientation	Mode		
	I	II	III
15º	60.85	71.94	**77.08**
45º	60.50	**67.83**	46.59
60º	**73.38**	66.18	61.66

Table 4
Computation time for terraces of different sizes.

$(a \times b)$	n_u	t
(30×10)	20	0.592
$\sqrt{10}(30 \times 10)$	256	4.508
$10(30 \times 10)$	2472	38.845
$20(30 \times 10)$	10143	154.379

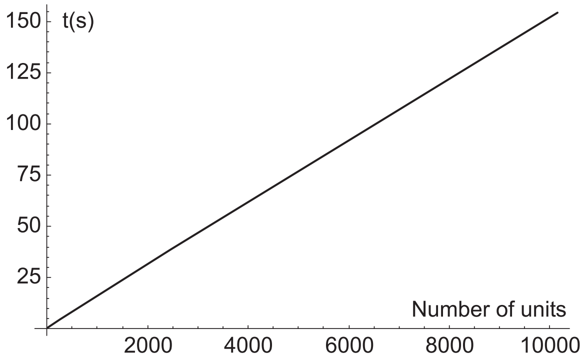

Fig. 14. Computation time as a function of n_u.

nates are the same for all the rectangles in the first row. The increase in the x coordinates between one rectangle and the next is given by:

$$\Delta x = \begin{cases} \dfrac{e_h}{\cos\alpha} + \dfrac{W}{\cos\alpha} & \text{if} \quad \alpha \neq \pi/2 \\ e_v + L & \text{if} \quad \alpha = \pi/2 \end{cases}; \quad \Delta y = 0$$

Thus, the coordinates of the four vertices A, B, C, and D of the rectangles in the first row are given by:

$$R_{1i}: \begin{cases} A(x_A + (i-1)\Delta x, y_A) & \rightarrow \quad D \\ B(x_B + (i-1)\Delta x, y_B) & \rightarrow \quad C \end{cases}; \quad i = 1, \ldots, n$$

From each rectangle in the first row, new rectangles R_{ji} are added in a direction parallel to the N–S direction, using the following relationships:

$$\delta x = \begin{cases} e_v \sin\alpha + L\sin\alpha & \alpha \neq \pi/2 \\ 0 & \alpha = \pi/2 \end{cases}; \quad \delta y = \begin{cases} e_v \cos\alpha + L\cos\alpha & \alpha \neq \pi/2 \\ e_v \sin\alpha + W\sin\alpha & \alpha = \pi/2 \end{cases}$$

$$R_{ji}: \begin{cases} A(x_A + (j-1)\delta x, y_A + (j-1)\delta y) & \rightarrow \quad D \\ B(x_B + (j-1)\delta x, y_B + (j-1)\delta y) & \rightarrow \quad C \end{cases}; \quad j = 1, \ldots, m$$

The packing pattern is completed by placing new rectangles R_{k1} $(k = 0, -1, \ldots)$ vertically aligned with the base rectangle R_{11}. The coordinates of the four vertices of rectangles R_{k1} are given by:

$$\Delta x = 0; \quad \Delta y = \begin{cases} \dfrac{e_h}{\sin\alpha} + \dfrac{W}{\sin\alpha} & \text{if} \quad \alpha \neq 0 \\ e_v + L & \text{if} \quad \alpha = 0 \end{cases}$$

$$R_{k1}: \begin{cases} A(x_A, y_A + (1-k)\Delta y) & \rightarrow \quad D \\ B(x_B, y_B + (1-k)\Delta y) & \rightarrow \quad C \end{cases}; \quad k = 0, -1, \ldots$$

Finally, from each rectangle R_{k1}, new rectangles are added in a direction parallel to the N–S direction.

TYPE (II) E-W ALIGNMENT

This second packing scheme consists in placing rows of reflectors parallel to the east–west direction. In this scheme (see Fig. 10), we define a base rectangle R_{11} using two vertices A and B, which are located as close as possible to the upper-right corner of the terrace. The coordinates of the four vertices A, B, C, and D are given by:

$$R_{11}: \begin{cases} A(eb, e'b + L\cos\alpha) & \rightarrow \quad D(x_A + W\cos\alpha, y_A + W\sin\alpha) \\ B(eb + L\sin\alpha, e'b) & \rightarrow \quad C(x_B + W\cos\alpha, y_B + W\sin\alpha) \end{cases}$$

Table 5
Computation time and optimal solution for different length steps.

l_s	ns_W	ns_L	$ns_W \cdot ns_L$	t	$L^* \times W^*$	r^*
0.1	5	5	25	0.514	2.1×1.4	0.2352
0.05	10	10	100	1.639	2.1×1.45	0.2436
0.01	50	50	2500	33.556	2.14×1.45	0.24824
0.005	100	100	10000	132.601	2.14×1.455	0.249096

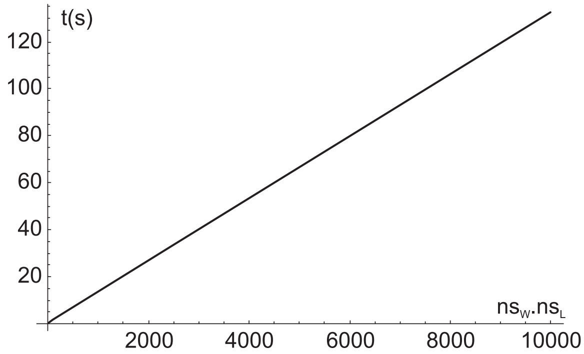

Fig. 15. Computation time as a function of $ns_W \cdot ns_L$.

First, the packing pattern of the first column is completed by placing vertically, from top to bottom, as many rectangles R_{1i} as possible. The increase of the y coordinates between one rectangle and the next is given by:

$$\Delta x = 0; \quad \Delta y = \begin{cases} \dfrac{e_v}{\cos\alpha} + \dfrac{L}{\cos\alpha} & \text{if} \quad \alpha \neq \pi/2 \\ e_h + W & \text{if} \quad \alpha = \pi/2 \end{cases}$$

Thus, the coordinates of the four vertices A, B, C, and D of the rectangles in the first column are given by:

$$R_{i1} : \begin{cases} A(x_A, y_A + (i-1)\Delta y) & \rightarrow & D \\ B(x_B, y_B + (i-1)\Delta y) & \rightarrow & C \end{cases}; \quad i = 1, \dots, n$$

From each rectangle in the first column, new rectangles R_{ij} are added in a direction perpendicular to the N–S direction, using the following relationships:

$$\delta x = \begin{cases} e_h \cos\alpha + W\cos\alpha & \alpha \neq \pi/2 \\ e_h \sin\alpha + L\sin\alpha & \alpha = \pi/2 \end{cases}; \quad \delta y = \begin{cases} e_h \sin\alpha + W\sin\alpha & \alpha \neq \pi/2 \\ 0 & \alpha = \pi/2 \end{cases}$$

$$R_{ij} : \begin{cases} A(x_A + (j-1)\delta x, y_A + (j-1)\delta y) & \rightarrow & D \\ B(x_B + (j-1)\delta x, y_B + (j-1)\delta y) & \rightarrow & C \end{cases}; \quad j = 1, \dots, m$$

The packing pattern is completed by placing new rectangles R_{k1} ($k = 0, -1, \dots$) horizontally aligned with the base rectangle R_{11}. The coordinates of the four vertices of rectangles R_{k1} are given by:

$$\Delta x = \begin{cases} \dfrac{e_v}{\sin\alpha} + \dfrac{L}{\sin\alpha} & \text{if} \quad \alpha \neq 0 \\ e_h + W & \text{if} \quad \alpha = 0 \end{cases}; \quad \Delta y = 0$$

$$R_{k1} : \begin{cases} A(x_A + (1-k)\Delta x, y_A) & \rightarrow & D \\ B(x_B + (1-k)\Delta x, y_B) & \rightarrow & C \end{cases}; \quad k = 0, -1, \dots$$

TYPE (III) X-Y ALIGNMENT

Finally, we present a third packing scheme, inspired by the classic method that inscribes irregular shapes into rectangles. This scheme consists in placing rows of reflectors parallel to the terrace edges and hence parallel to our reference axes $(x-y)$. We once again define a base rectangle R_{11} close to the bottom-right corner of the terrace:

$$R_{11} : \begin{cases} A(eb, e'b + W\sin\alpha) & \rightarrow & D(x_A + L\sin\alpha, y_A + L\cos\alpha) \\ B(eb + W\cos\alpha, e'b) & \rightarrow & C(x_B + L\sin\alpha, y_B + L\cos\alpha) \end{cases}$$

Depending on the parameters of the problem, the distance between reflectors on the x-axis can be given by e_h (case III-A) or by e_v (case III-B), and the distance between reflectors on the y-axis can be given by e_v (case III-A) or by e_h (case III-B). These two cases, III-A and III-B, are shown in Figs. 11 and 12, respectively.

(III-A) In case III-A, the coordinates of the vertices of the rectangles are calculated as follows.

$$R_{1i}: \begin{cases} A(x_A + (i-1)\Delta x, y_A) & \rightarrow & D \\ B(x_B + (i-1)\Delta x, y_B) & \rightarrow & C \end{cases}; \quad i = 1, \ldots$$

$$\Delta x = \begin{cases} \dfrac{e_h}{\cos\alpha} + \dfrac{W}{\cos\alpha} & \text{if} \quad \alpha \neq \pi/2 \\ e_v + L & \text{if} \quad \alpha = \pi/2 \end{cases}; \quad \Delta y = 0$$

$$R_{i1}: \begin{cases} A(x_A, y_A + (i-1)\Delta y) & \rightarrow & D \\ B(x_B, y_B + (i-1)\Delta y) & \rightarrow & C \end{cases}; \quad i = 1, \ldots$$

$$\Delta x = 0; \quad \Delta y = \begin{cases} \dfrac{e_v}{\cos\alpha} + \dfrac{L}{\cos\alpha} & \text{if} \quad \alpha \neq \pi/2 \\ e_h + W & \text{if} \quad \alpha = \pi/2 \end{cases}$$

(**III-B**) In case III-B, the coordinates of the vertices of the rectangles are calculated as follows.

$$R_{1i}: \begin{cases} A(x_A + (i-1)\Delta x, y_A) & \rightarrow & D \\ B(x_B + (i-1)\Delta x, y_B) & \rightarrow & C \end{cases}; \quad i = 1, \ldots$$

$$\Delta x = \begin{cases} \dfrac{e_v}{\sin\alpha} + \dfrac{L}{\sin\alpha} & \text{if} \quad \alpha \neq \pi/2 \\ e_h + W & \text{if} \quad \alpha = \pi/2 \end{cases}; \quad \Delta y = 0$$

$$R_{i1}: \begin{cases} A(x_A, y_A + (i-1)\Delta y) & \rightarrow & D \\ B(x_B, y_B + (i-1)\Delta y) & \rightarrow & C \end{cases}; \quad i = 1, \ldots$$

$$\Delta x = 0; \quad \Delta y = \begin{cases} \dfrac{e_h}{\sin\alpha} + \dfrac{W}{\sin\alpha} & \text{if} \quad \alpha \neq \pi/2 \\ e_v + L & \text{if} \quad \alpha = \pi/2 \end{cases}$$

5. Numerical examples

This section shows the results obtained with the three types of packing described in the previous section. The optimization algorithm was implemented using the commercial software Mathematica^{TM}.

As stated in Section 1 (Introduction), a prototype with these characteristics has been manufactured at a vocational training school (CIFP-Mantenimiento y Servicios a la Producción) in La Felguera, Asturias, Spain. The values considered for the upper and lower bounds of the reflector dimensions (width and length) are based on the actual dimensions of the prototype: $W^{min} = 1.0$ (m); $W^{max} = 1.5$ (m); $L^{min} = 2.0$ (m); $L^{max} = 2.5$ (m). Other authors have used similar dimensions [52].

We consider, without loss of generality, that $e_h = e_v = 1.0$ (m), and $eb = e'b = 1.0$ (m). With regard to the dimensions of the terrace (a) and (b), we analyse a square case ($F_r = 1$), and also two rectangular cases ($F_r = 2$, and $F_r = 3$). In addition, the influence of the orientation of the terrace is taken into account, varying the angle that the terrace forms with the north-south direction between 0 and 90^o.

The algorithm finds, for each packing scheme, the reflector dimensions (width and length) which maximize the total mirror field area. The optimization procedure is in fact a brute force algorithm that evaluates all the possible combinations of width and length between their upper and lower bounds, using a length step, l_s, of 0.1 (m). Nevertheless, the algorithm running time is about 1 s on a personal computer (Intel Core 2/2.66 GHz).

The optimal solutions, for each packing scheme (I, II, and III), are shown in Table 2. The packing scheme that gives the best result is highlighted using bold typeface. The value shown in this table is the ratio r of the total mirror field area to the total area of the terrace:

$$r = \frac{A_T}{a \cdot b}$$

According to these results, the packaging scheme that gives the best solution depends on the angle of orientation of the terrace. Obviously, when the angle is 0^o or 90^o, the three packing schemes give the same optimal solution. When the angle is less than 15^o or greater than 75^o, the best packing scheme is Type III. However, when the angle is between 30^o and 60^o , the best packing scheme is Type I or Type II.

As an example, Fig. 13 shows the optimal configurations for a terrace of dimensions $a \times b = 20 \times 10$ (m), with an angle of orientation of 15^o (III mode), 45^o (II mode), and 60^o (I mode). Each configuration shows in the upper part the optimal values of the parameters; namely, from top to bottom: length (L), width (W), r, and number of reflectors (n_u).

Table 3 shows the energy absorbed by the absorber tube per year, for the optimal configurations depicted in Fig. 13. All the calculations are based on a sub-hourly distribution of direct normal irradiance in a specific geographic location: Almeria (Spain), with latitude 36^{o}50′07″N, longitude 02^{o}24′08″W, and altitude 22 (m). Derived database and system integrating

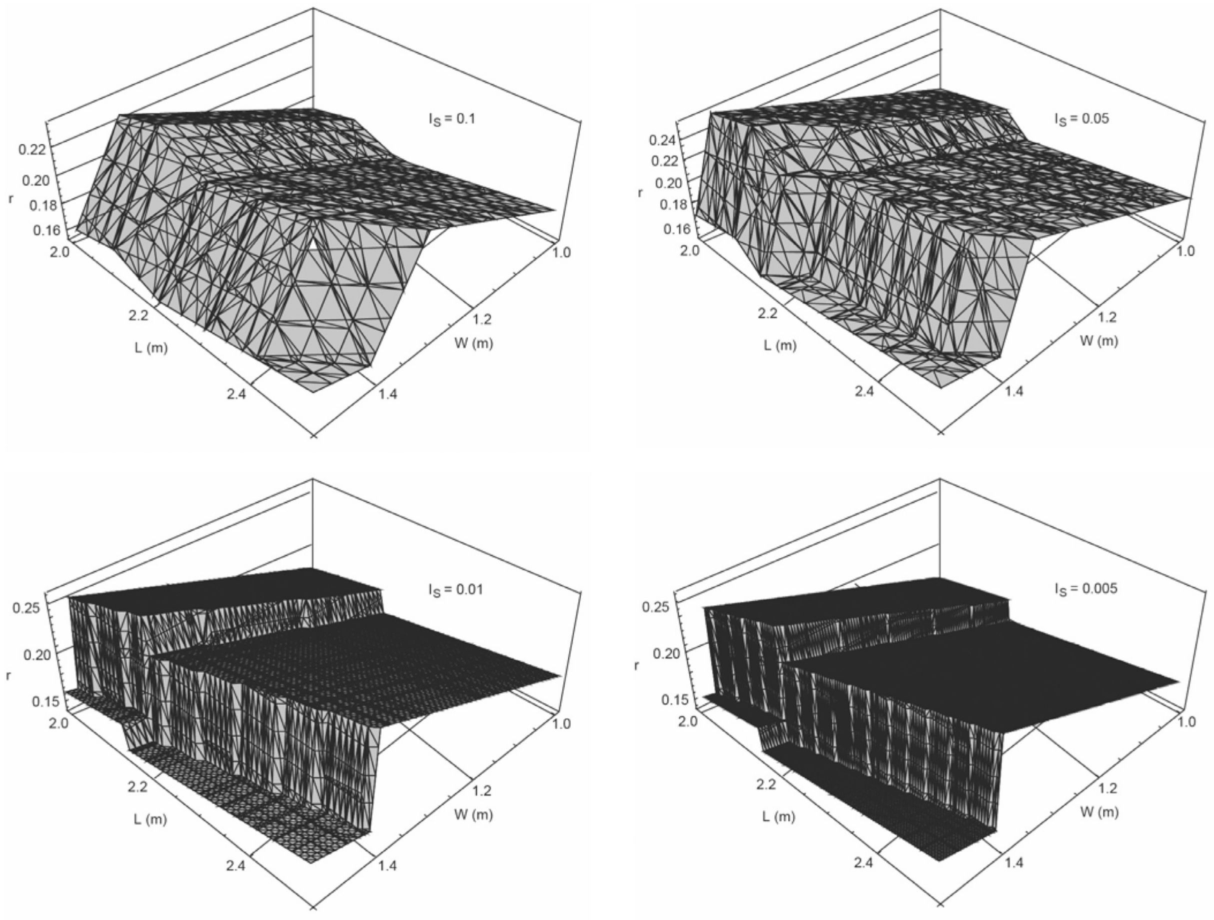

Fig. 16. Value of r as a function of L and W for each l_s.

data [53] have been used to estimate the solar irradiance. Numerical simulations were performed using a MATLAB code [35] which incorporates subroutines, discretized every 10 min, to calculate: *DNI*, mirror position, *IAM*, l_{ciai}, and l_a. The effects of shading, blocking, and end loss have also been taken into account.

5.1. Time efficiency and convergence

Although the algorithms presented in this paper were developed for this specific application (the installation of SSLFRs on building roofs), we believe that they could also be useful in problems with similar characteristics. In an application where the number of units to be installed is very high, the computation time of the algorithms is a factor that has to be taken into account.

Table 4 and Fig. 14 show the computation time (t) in seconds as a function of the optimal number of reflectors (n_u) for terraces of different sizes. This analysis has been carried out using the following values: $\alpha = 30^o$, $l_s = 0.1(\mathrm{m})$, $F_r = 3$. The results shown correspond to Type (III) algorithm, yet the other algorithms give similar figures. As can be seen in Fig. 14, the computation time grows linearly with the optimal number of reflectors: $O(n_u)$. Since no potential or exponential growth is obtained, the algorithms could also be used for large-scale problems.

In addition to the size of the terrace, another factor that determines the computation time is the discretization size or length step (l_s) used to evaluate all the possible combinations of width (W) and length (L) between their upper and lower bounds. Table 5 and Fig. 15 show the computation time (t) in seconds as a function of the number of discretization subintervals considered for W (ns_W) and L (ns_L). This analysis was carried out using the following values: $\alpha = 60^o$, $a \times b = 30 \times 10(\mathrm{m})$, $W^{\min} = 1(\mathrm{m})$, $W^{\max} = 1.5(\mathrm{m})$, $L^{\min} = 2(\mathrm{m})$, $L^{\max} = 2.5(\mathrm{m})$. With the lower and upper bounds considered here, $ns_W = ns_L$, though, obviously, these values could be different. As in the previous case, the results shown correspond to the Type (III) algorithm, and the other algorithms also give similar figures. As can be seen in Fig. 15, the computation time also grows linearly with the product of discretization subintervals: $O(ns_W \cdot ns_L)$.

Table 5 shows also the optimal values of length (L^*), width (W^*), and ratio (r^*) as a function of the length step. By decreasing the length step, the solution quickly converges to its optimal value. The optimal number of reflectors is 24, regardless of the length step value.

Fig. 16 shows the value of r as a function of L and W for each of the length step values considered. This figure was produced using Mathematica® via a polynomial interpolation of the values obtained with the algorithm. Obviously, the accuracy depends on the value of the length step. As the length step decreases, the graph approaches a step function.

6. Conclusions

This paper presents a mathematical method to optimize the installation of small scale linear Fresnel reflectors in urban residential buildings. The influence of the form and orientation of the available roof area is analysed in order to determine the optimal number and arrangement of the reflectors. Shadowing effects are also taken into account. The optimization procedure considers three new packing algorithms, developed specifically for this problem. The results show that the algorithm which provides the best solution depends on the characteristics of each particular problem, i.e., the dimensions and orientation of the terrace, and the values considered for the upper and lower bounds of the reflector dimensions (width and length).

The obtained algorithms could also be useful in other applications with similar characteristics. It has been shown that they could be applied to large-scale problems with very reasonable computing times, given that the computing time grows linearly with the optimal number of reflectors and with the discretization size. The precision of the algorithms depends on the discretization size. The algorithms presented in this paper converge quickly to the optimal solution and are hence a viable alternative bearing in mind that the optimal solution cannot be obtained using conventional methods of differential calculus.

The presented algorithms can be generalized to the study of terraces of irregular form (as a composition of several rectangles). Other possible refinements of the optimization method could be the analysis of some components that are usually found on building roofs: elevator machine rooms, fans, et cetera.

Acknowledgments

We wish to thank M. F. Fanjul, head of the CIFP-Mantenimiento y Servicios a la Producción vocational training school in La Felguera, Asturias, Spain, and the teachers L. Rodríguez and F. Salguero for their work on the (on-going) building of the prototype for the design presented in this paper.

References

[1] 2014. United Nations. World Urbanization Prospects: Revision 2014.
[2] 2010. Directive 2010/31/EC. On the Energy Performance of Buildings.
[3] 2009. Directive 2009/28/EC. On the promotion of the use of energy from renewable sources.
[4] 2002. Directive 2002/91/EC. On the Energy Performance of Buildings.
[5] A. Mariaud, S. Acha, N. Ekins-Daukes, N. Shah, C.N. Markides, Integrated optimisation of photovoltaic and battery storage systems for UK commercial buildings, Appl. Energy 199 (2017) 466–478.
[6] S. Kalogirou, Solar thermal collectors and applications, Prog. Energy Combust. Sci. 30 (2004) 231–295.
[7] S. Kalogirou, The potential of solar industrial process heat applications, Appl. Energy 76 (2003) 337–361.
[8] F. Motte, G. Notton, C. Cristofari, J.L. Canaletti, Design and modelling of a new patented thermal solar collector with high building integration, Appl. Energy 102 (2013) 631–639.
[9] L. Navarro, A. Gracia, S. Colclough, M. Browne, S.J. McCormack, P. Griffiths, L.F. Cabeza, Thermal energy storage in building integrated thermal systems: A review. part 1. active storage systems, Renew. Energy 88 (2016) 526–547.
[10] C. Good, I. Andresen, A.G. Hestnes, Solar energy for net zero energy buildings – a comparison between solar thermal, PV and photovoltaic–thermal (PV/t) systems, Solar Energy 122 (2015) 986–996.
[11] G. Tsalikis, G. Martinopoulos, Solar energy systems potential for nearly net zero energy residential buildings, Solar Energy 115 (2015) 743–756.
[12] T. Sultana, G.L. Morrison, G. Rosengarten, Thermal performance of a novel rooftop solar micro-concentrating collector, Solar Energy 86 (2012) 1992–2000.
[13] T. Sultana, G.L. Morrison, R.A. Taylor, G. Rosengarten, Numerical and experimental study of a solar micro concentrating collector, Solar Energy 112 (2015) 20–29.
[14] P. Bermejo, F.J. Pino, F. Rosa, Solar absorption cooling plant in seville, Solar Energy 84 (2010) 1503–1512.
[15] N. Velázquez, O. García-Valladares, D. Sauceda, R. Beltrán, Numerical simulation of a linear Fresnel reflector concentrator used as direct generator in a solar-GAX cycle, Energy Convers. Manag. 51 (2010) 434–445.
[16] M.J. Montes, C. Rubbia, R. Abbas, J.M. Martínez-Val, A comparative analysis of configurations of linear Fresnel collectors for concentrating solar power, Energy 73 (2014) 192–203.
[17] D. Mills, G.L. Morrison, Compact linear Fresnel reflector solar thermal powerplants, Solar Energy 68 (2000) 263–283.
[18] R. Abbas, J. Muñoz, J.M. Martínez-Val, Steady-state thermal analysis of an innovative receiver for linear Fresnel reflectors, Appl. Energy 92 (2012) 503–515.
[19] R. Abbas, M.J. Montes, M. Piera, J.M. Martínez-Val, Solar radiation concentration features in linear Fresnel reflector arrays, Energy Convers. Manag. 54 (2012) 133–144.
[20] A. Barbón, N. Barbón, L. Bayón, J.A. Otero, Theoretical elements for the design of a small scale linear fresnel reflector: frontal and lateral views, Solar Energy 132 (2016) 188–202.
[21] A. Barbón, N. Barbón, L. Bayón, J.A. Otero, Optimization of the length and position of the absorber tube in small-scale linear fresnel concentrators, Renew. Energy 99 (2016) 986–995.
[22] B. Giffith, P. Torcellini, N. Long, Assessment of the technical potential for achieving zero-energy commercial buildings, in: Proceedings of the ACEEE Summer Study Pacific Grove, 2006.

[23] S. Izquierdo, M. Rodrigues, N. Fueyo, A method for estimating the geographical distribution of the available roof surface area for large-scale photovoltaic energy-potential evaluations, Solar Energy 82 (2008) 929–939.
[24] K. Mainzer, K. Fath, R. McKenna, J. Stengel, W. Fichtner, F. Schultmann, A high-resolution determination of the technical potential for residential-roof–mounted photovoltaic systems in Germany, Solar Energy 105 (2014) 715–731.
[25] L. Bergamasco, P. Asinari, Scalable methodology for the photovoltaic solar energy potential assessment based on available roof surface area: application to piedmont region (Italy), Solar Energy 85 (2011) 1041–1055.
[26] Y. Li, D. Ding, C. Liua, C. Wang, A pixel-based approach to estimation of solar energy potential on building roofs, Energy Build. 129 (2016) 563–573.
[27] L. Martin, L. March (Eds.), Urban Space and Structures, Cambridge University Press, UK, 1972.
[28] K. Steemers, N. Baker, D. Crowther, J. Dubiel, M.H. Nikolopoulou, C. Ratti, City texture and microclimate, Urb. Des. Stud. 3 (1997) 25–50.
[29] I. Reda, A. Andreas, Solar position algorithm for solar radiation applications, in: Technical Report NREL/TP-560-34302, Colorado, USA, 2008.
[30] P.H. Theunissen, W.A. Beckman, Solar transmittance characteristics of evacuated tubular collectors with diffuse back reflectors, Solar Energy 35 (1985) 311–320.
[31] M. Binotti, G. Manzolini, G. Zhu, An alternative methodology to treat solar radiation data for the optical efficiency estimate of different types of collectors, Solar Energy 110 (2014) 807–817.
[32] M.A. Moghimi, K.J. Craig, J.P. Meyer, A novel computational approach to combine the optical and thermal modelling of linear fresnel collectors using the finite volume method, Solar Energy 116 (2015) 407–427.
[33] J.A. Duffie, W.A. Beckman, Solar Engineering of Thermal Processes, fourth ed., John Wiley & Sons, New York, 2013.
[34] V.M. Sharma, J.K. Nayak, S.B. Kedare, Comparison of line focusing solar concentrator fields considering shading and blocking, Solar Energy 122 (2015) 924–939.
[35] A. Barbón, N. Barbón, L. Bayón, J.A. Sánchez-Rodríguez, Parametric study of the small scale linear fresnel reflector, Renew. Energy 116 (2018) 64–74.
[36] S. Gadsden, M. Rylatt, K. Lomas, D. Robinson, Predicting the urban solar fraction: a methodology for energy advisers and planners based on GIS, Energy Build. 35 (2003) 37–48.
[37] L.K. Wiginton, H.T. Nguyen, J.M. Pearce, Quantifying rooftop solar photovoltaic potential for regional renewable energy policy, Comput. Environ. Urb. Syst. 34 (2010) 345–357.
[38] H. Bryan, H. Rallapalli, J.J. Ho, Designing a solar ready roof: establishing the conditions for a high-performing solar installation, in: Proceedings of the Thirty-Ninth ASES National Solar Conference, 5, 2010, pp. 4081–4110.
[39] MVIV. Ministry of Housing (Spanish Government), Technical Building Code (RD 314/2006, March 17th); Basic Document: Basic health safety (HS) requirements. 2009.
[40] Spanish Technical Building Code Royal Decree 314/2006 of 17 March 2006.
[41] H. Dyckhoff, A typology of cutting and packing problems, Eur. J. Oper. Res. 44 (1990) 145–159.
[42] S. Imahori, M. Yagiura, H. Nagamochi, Practical algorithms for two-dimensional packing, department of mathematical informatics, in: University of Tokyo METR2006-19, 2006.
[43] E.G. Coffman, M.R. Garey, D.S. Johnson, Approximation algorithms for bin-packing - a survey, in: D.S. Hochbaum (Ed.), Approximation Algorithms for Bin Packing for NP-Hard Problems, PWS Publishing Company, Boston, 1997, pp. 46–93.
[44] A. Lodi, S. Martello, D. Vigo, Heuristic and metaheuristic approaches for a class of two-dimensional bin packing problems, INFORMS J. Comput. 11 (1999) 345–357.
[45] S. Martello, P. Toth, in: Knapsack Problems: Algorithms and Computer Implementations, Wiley and Sons, Chichester, 1990.
[46] Y.L. Wu, W. Huang, S. Lau, C.K. Wong, G.H. Young, An effective quasi-human based heuristic for solving the rectangle packing problem, Eur. J. Oper. Res. 141 (2002) 341–358.
[47] P.C. Gilmore, R.E. Gomory, Multistage cutting stock problems of two and more dimensions, Oper. Res. 13 (1965) 94–120.
[48] R.A. Valdes, A. Parajon, J.M. Tamarit, A tabu search algorithm for large-scale guillotine (un)constrained two-dimensional cutting problems, Comput. Oper. Res. 29 (2002) 925–947.
[49] F. Vanderbeck, A nested decomposition approach to a three-stage, two-dimensional cutting-stock problem, Manag. Sci. 47 (2001) 864–879.
[50] R. Morabito, S. Morales, A simple and effective recursive procedure for the manufacturer's pallet loading problem, J. Oper. Res. Soc. 49 (1998) 819–828.
[51] E.G. Birgin, R.D. Lobato, R. Morabito, An effective recursive partitioning approach for the packing of identical rectangles in a rectangle, J. Oper. Res. Soc. 61 (2010) 306–320.
[52] Y. Zhu, J. Shi, Y. Li, L. Wang, Q. Huang, G. Xu, Design and thermal performances of a scalable linear fresnel reflector solar system, Energy Convers. Manag. 146 (2017) 174–181.
[53] Andalusian Energy Agency (AEA). https://www.agenciaandaluzadelaenergia.es.